Evidence of multicenter structure of cerium ions in gadolinium gallium garnet crystals studied by infrared absorption spectroscopy

H. Przybylińska,[1] Chong-Geng Ma,[2] M. G. Brik,[2] A. Kamińska,[1] J. Szczepkowski,[1] P. Sybilski,[1] A. Wittlin,[1,3] M. Berkowski,[1] W. Jastrzębski,[1] and A. Suchocki[1,4]

[1]*Institute of Physics, Polish Academy of Sciences, Al. Lotników 32/46, 02-668 Warsaw, Poland*

[2]*Institute of Physics, University of Tartu, Riia 142, Tartu 51014, Estonia*

[3]*Cardinal Stefan Wyszyński University in Warsaw, ul. Dewajtis 5, 01-815 Warsaw, Poland*

[4]*Institute of Physics, Kazimierz Wielki University, Weyssenhoffa 11, 85-072 Bydgoszcz, Poland*

(Received 20 August 2012; revised manuscript received 5 January 2013; published 16 January 2013)

Low temperature, infrared absorption spectra of gadolinium gallium garnet crystals doped with Ce are presented. In the region of intraconfigurational $4f$-$4f$ transitions the spectra exhibit existence of at least two different, major Ce^{3+} related centers in the GGG crystals and also some other centers at lower concentration. The spectrum of $4f$-$4f$ intrashell transitions of Ce^{3+} ions extends up to about 3700 cm^{-1} due to the large splitting of the $^2F_{7/2}$ excited state. In the visible region the absorption spectrum shows influence of symmetry-related selection rules. The absorption coefficient changes in the region of $4f^1$-$5d^1$ transitions due to thermal population of the second level, belonging to the $^2F_{5/2}$ ground state. This suggests that the symmetry of the site occupied by Ce^{3+} ions, which substitute Gd^{3+}, is higher than D_2 expected for garnet hosts.

DOI: 10.1103/PhysRevB.87.045114 PACS number(s): 78.40.Ha, 71.70.Ch, 71.20.Eh

I. INTRODUCTION

Cerium doped materials are the subject of numerous studies for solid state laser materials,[1,2] phosphors,[3–8] and scintillators.[9,10] Ce^{3+} has the simplest of the $4f^n$ ground state configurations ($n = 1$) and in many compounds it exhibits broadband emission originating from parity allowed interconfigurational $4f^05d^1 \rightarrow 4f^15d^0$ transitions. It is also studied for better understanding of $d \leftrightarrow f$ absorption and luminescence processes, both experimentally[11–13] and theoretically.[14–16] The special importance of Ce^{3+} ions among the lanthanides comes from the fact that the splitting of $5d$ states of cerium can be extrapolated and used for the analysis of f-d spectra of other rare-earth ions.

Gadolinium gallium garnet (GGG) doped with some rare-earth ions is an important laser material.[17,18] Its optical properties are also studied upon doping with various transition-metal ions.[19–22] The crystal structure of GGG is described by the $Ia3d$ space group (No. 230) and there are eight formula units in one cubic unit cell with the lattice constant 12.3829 Å.[23] Ce^{3+} ions doped in GGG substitute Gd^{3+} ions in sites eightfold coordinated with oxygen ions in D_2 point-group symmetry, as shown in Fig. 1. The geometrical figure formed by the GdO_8 molecule can be viewed as a highly distorted cube (each side of this cube is divided into two triangles, tilted slightly against each other). More detailed inspection of the nearest neighborhood of the Ce^{3+} dopant demonstrates that there are two kinds of oxygen ions (hereafter, termed O1 and O2) with different interionic distances R(Ce-O1) = 2.35842 Å and R(Ce-O2) = 2.47268 Å. Such a local coordination environment is similar to that of Ce^{3+} ions in the well-known $Y_3Al_5O_{12}$ (YAG) reported in Fig. 1 of Ref. 24, suggesting that the optical properties of Ce^{3+} ions in YAG may be regarded as a good reference for our system.

As it has been shown in Ref. 25, the distances between the central rare-earth (RE) ion and the two nonequivalent surrounding oxygen ions are a function of pressure in GGG crystal. For this crystal at a pressure of ∼11.8 GPa the distances between the central Gd and all surrounding oxygen ions become approximately equal to each other. The dodecahedron surrounding the central RE ion in GGG host is transformed into a polyhedron with two opposite slightly rectangular (not square-shaped) faces, which are parallel to each other but twisted around the vertical axis. Each of the four other faces still forms two triangles (typical for the REO_8 dodecahedron in a garnet structure). The shape of this figure (similar to a square antiprism) has a symmetry close to D_{2d} (higher than D_2 symmetry, and closer to cubic); although it still can be viewed as a distorted cube. The approximate picture of the GdO_8 molecule at a pressure of 11.8 GPa is shown in Fig. 3 of Ref. 25. Substitution of Gd^{3+} ion with Ce^{3+} can lead to the similar effects as application of pressure.

In some garnets Ce^{3+} ions form very efficient luminescence centers, in the others the luminescence is absent due to nonradiative energy transfer processes. $Y_3Al_5O_{12}$ (YAG) belongs to the first group of garnet crystals, while $Gd_3Ga_5O_{12}$ (GGG) and $Y_3Ga_5O_{12}$ (YGG) garnets represent the second one.[26]

The electronic energy structure of Ce^{3+} ions with $4f^1$ configuration has a $^2F_{5/2}$ ground state and a $^2F_{7/2}$ excited state. Crystal field (CF) and spin-orbit interactions split these two states, although it is common to present these states as two levels separated by about 2200 cm^{-1}, as in the classic Dieke diagram.[27] Luminescence studies of $d \leftrightarrow f$ transitions often support this picture since the luminescence spectra can be deconvoluted into two semi-Gaussian bands separated by about 2000 cm^{-1}.[26] On the other hand, an old paper by Herrmann *et al.* reports a large splitting of the Ce^{3+} excited level in the yttrium gallium garnet explained with theoretical analysis including states of D_2 and cubic symmetry.[14]

It is well known that multicenters[28] of rare-earth and transition metal ions occur often in garnets. It is associated with structural imperfection of these materials, such as existence of so-called antisites, exchange of cations between dodecahedral and octahedral sites,[29] nonstoichiometry, and other defects

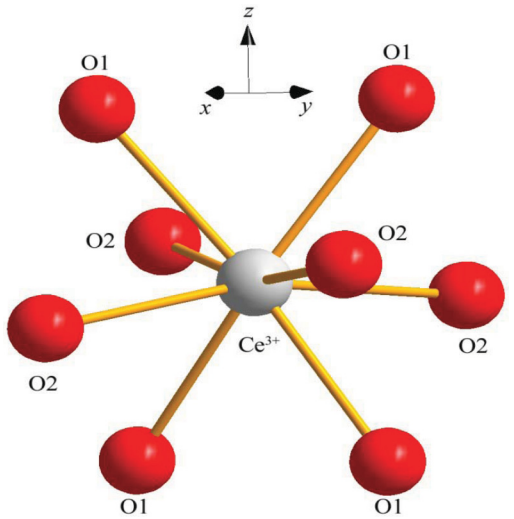

FIG. 1. (Color online) Schematic representation of the local coordination structure of Ce^{3+} occupying the site of Gd^{3+} in GGG.

existing in the crystal structure of garnets. However, there is a shortage of information on the structure of Ce^{3+} multicenters in garnets. The zero-phonon lines of $d \leftrightarrow f$ transitions are weak, if not completely quenched, due to strong electron-lattice interaction and a large Huang-Rhys factor. Nevertheless, a recent paper by Feofilov *et al.*[30] shows some indirect evidence of Ce^{3+} multisite structure in YAG crystal.

In this paper we present direct evidence of multisite structure of Ce-doped GGG crystals. The low-temperature, far-infrared absorption measurements show that the splitting of the excited $^2F_{7/2}$ level is very large and extends up to about 4000 cm^{-1}. The theoretical crystal field analysis supports our experimental findings.

Both experimental and theoretical studies of the $4f$-$4f$ and $4f$-$5d$ absorption transitions of Ce^{3+} ions in GGG presented here show the importance of site symmetry and the resulting selection rules for the analysis of Ce^{3+} optical properties. For example, these factors strongly influence the temperature changes of the *f-d* absorption coefficients.

II. EXPERIMENTAL DETAILS

Several GGG crystals, pure and doped with Ce, were grown by the Czochralski method. The Ce content of doped crystals was 0.5, 1.2, and 5 at.%. The far-infrared absorption spectra were measured with a VERTEX 80v (Bruker) and a BOMEM DA3 FTIR Fourier-transformed infrared (FTIR) spectrophotometer. For low temperature measurements the samples were placed into an Oxford Instruments CF-102 continuous-flow cryostat equipped with KBr windows. Spectral resolution of the measurements was 2 and 1 cm^{-1} for low and room temperature measurements, respectively.

III. EXPERIMENTAL RESULTS

A. Ce^{3+} $4f$-$4f$ absorption spectra

Room-temperature absorption spectra of pure GGG crystal and GGG:Ce^{3+} (0.5% and 5%) crystals in the region of cerium $4f$-$4f$ intraconfigurational transitions are presented in Fig. 2.

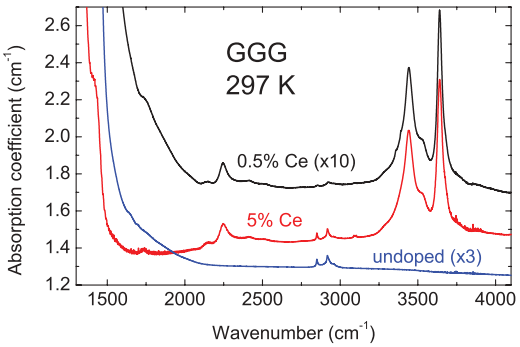

FIG. 2. (Color online) Absorption spectra of undoped and Ce-doped GGG crystals at room temperature in the region of intraconfigurational $4f \rightarrow 4f$ transitions. The 0.5% Ce spectrum is multiplied by 10, the spectrum of the undoped crystal is multiplied by 3.

They show two groups of lines associated with Ce^{3+} in the region of 2100–2600 cm^{-1} and between 3200 and 3800 cm^{-1}. The intensity of these lines is proportional to the Ce content in the samples. The group of sharp lines around 2800 cm^{-1}, which are also present in the undoped sample, is apparently not associated with Ce^{3+} and their origin is unknown. The strong reflection below 1500 cm^{-1} is due to Reststrahlen effects.

The transmission spectrum of the GGG:Ce (1.2%) sample, taken at 25 K, is presented in Fig. 3. A spurious background, associated most probably with interferences induced by a thin film accidentally deposited on the sample surfaces during cooling, was subtracted from the spectra.

There are two groups of lines clearly visible in the spectra: The first between 2100 and 2500 cm^{-1}, consisting of at least six lines, and the second around 3650 cm^{-1}. The second group contains two dominant lines with some additional, partly resolved structure. An expanded view of these two groups of lines is shown in Figs. 4(a) and 4(b).

The ground $^2F_{5/2}$ and excited $^2F_{7/2}$ states of Ce^{3+} ions in D_2 symmetry sites should be split into three and four levels, respectively. Since only the lowest component of the ground state is populated at low temperature, the observed transitions are from that state to the different components of the excited $^2F_{7/2}$ states. The number of lines observed in the spectra testifies that Ce^{3+} ions form at least two different major centers in GGG crystals. Some sites with apparently lower concentration contribute also to the spectra.

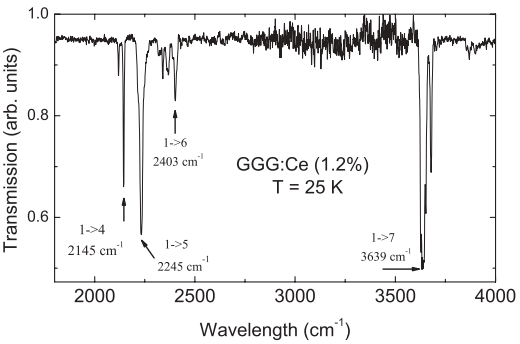

FIG. 3. Transmission spectrum of the GGG:Ce (1.2%) sample taken at 25 K in the region of Ce^{3+} $4f$-$4f$ transitions. Transitions designation and their energies are marked on the graph.

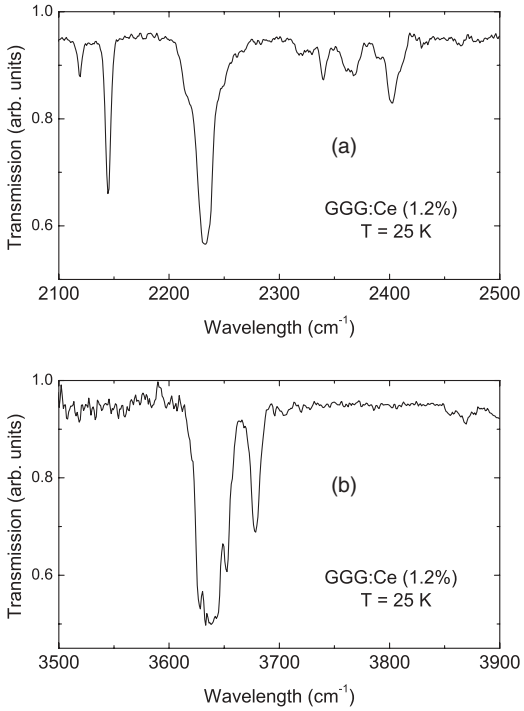

FIG. 4. (a) and (b) Expanded transmission spectra in the regions of Ce^{3+} 4*f*-4*f* absorption of GGG:Ce (1.2%), measured at 25 K.

Comparison of the room and low temperature spectra proves that the line peaked at 3442 cm^{-1} in the room temperature spectrum and absent at low temperature is a so-called "hot" line. It occurs due to thermal population of the second upper level of the $^2F_{5/2}$ ground multiplet, separated from the lowest level by about 200 cm^{-1}. The other hot lines associated with the transitions to the lower-lying levels of the $^2F_{7/2}$ state overlap either with the other 4*f*-4*f* transitions or with the beginning of the Reststrahlen band. Therefore they are less pronounced in the spectra.

B. Temperature dependence of the $4f$-$5d$ absorption spectra of Ce^{3+}

The temperature dependence of the absorption spectrum of the GGG:Ce crystal in the region of cerium *f*-*d* interconfigurational transitions is shown in Fig. 5, along with the theoretical simulation of the spectra described in the theoretical part of the paper (Secs. IV C and V).

The absorption spectra consist of two relatively broad absorption bands at all temperatures, with maxima at 426 and 346 nm (at 10 K). The intensity of the absorption band peaked at 346 nm gradually increases with increasing temperature at the expense of the absorption band at 426 nm. In addition to the broad absorption bands associated with *f*-*d* transitions of Ce^{3+} ions, there are sharp lines in the region between 315 and 270 nm, attributed to intrashell $4f$-$4f$ transitions of Gd^{3+} ions. These lines can be assigned to transitions from the ground $^8S_{7/2}$ state to the excited ^6P and ^6I terms, respectively. The strong absorption edge at about 225 nm is due to the valence-conduction band transitions of the host crystal. Figure 6 shows the temperature dependence of the relative value of the dipole matrix element M,[31] calculated for the 426

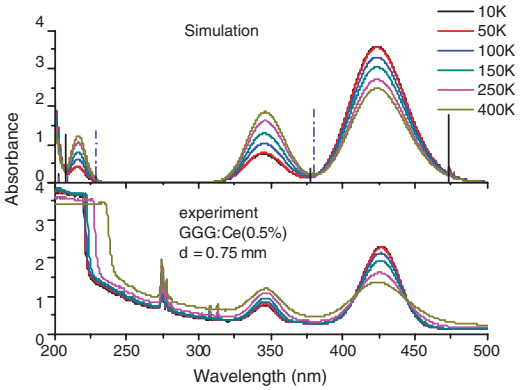

FIG. 5. (Color online) The temperature dependence of the simulated and observed absorption spectrum of the GGG:Ce (0.5%) crystal in the region of interconfigurational $4f \rightarrow 5d$ transitions at temperatures between 10 and 400 K. Only a few of the measured and calculated spectra are shown for clarity of the graph. The solid and dashed vertical bars represent the calculated energy positions and oscillator strengths of the zero-phonon lines for the transitions from the lowest two energy levels of the $4f^1$ configuration to the levels of the $5d^1$ configuration.

and 346 nm bands with

$$M = \int \alpha\omega \, d\omega, \tag{1}$$

where α is the absorption coefficient, and ω is the frequency of the light.

The 426 and 346 nm bands (marked here by their maxima at 10 K) are thermally deactivated and activated, respectively, which is associated with thermal population of the upper-lying sublevel of the $^2F_{5/2}$ ground state. The transitions to the two sublevels of the $5d$ state from these two sublevels of the $^2F_{5/2}$ ground state occur with different probabilities, which are associated with the selection rules. Therefore, the thermal population of the higher-lying level of the $^2F_{5/2}$ ground state changes the absorption coefficients in these absorption bands. Activation energies calculated from the decrease of the matrix element of the dipole transitions corresponding to the 426 nm band and increase of the one corresponding to the 346 nm

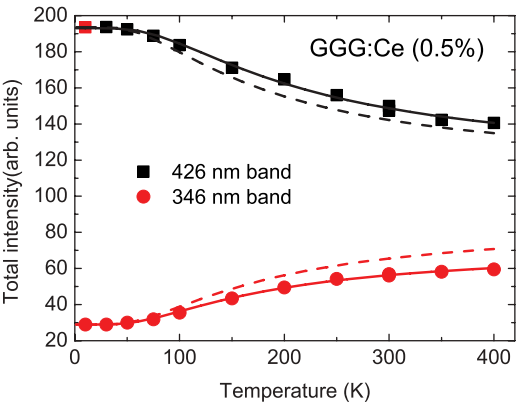

FIG. 6. (Color online) Temperature dependence of the dipole matrix element for two *f*-*d* transition bands of GGG:Ce (0.5%). The solid lines are computer fits of Eqs. (12) to the data, the broken lines are theoretical simulations (see Sec. V C for explanation).

band, obtained from the computer fit of Eqs. (12) are equal to (193 ± 10) and (162 ± 6) cm^{-1}, respectively. These energies are very close to each other, confirming the validity of the proposed model of the origin of these absorption bands.

IV. THEORETICAL

A. Parametrized Hamiltonians of $4f^1$ and $5d^1$ configurations

Since the Ce^{3+} ions replace Gd^{3+} ions in the GGG host with the site symmetry of D_2[xxiii], then using the standard notation of Wybourne[32] and Table 1.7 of Ref. 33 the parametrized effective Hamiltonians for the $4f^1$ and $5d^1$ configurations of Ce^{3+} ions in GGG can be respectively written as

$$\begin{aligned}\mathbf{H}(4f^1) = {} & E_{\text{avg}} + \zeta_{4f} s_f \cdot l_f + B_0^2(f)\mathbf{C}_0^{(2)} \\ & + B_2^2(f)\left(\mathbf{C}_2^{(2)} + \mathbf{C}_{-2}^{(2)}\right) + B_0^4(f)\mathbf{C}_0^{(4)} \\ & + B_2^4(f)\left(\mathbf{C}_2^{(4)} + \mathbf{C}_{-2}^{(4)}\right) + B_4^4(f)\left(\mathbf{C}_4^{(4)} + \mathbf{C}_{-4}^{(4)}\right) \\ & + B_0^6(f)\mathbf{C}_0^{(6)} + B_2^6(f)\left(\mathbf{C}_2^{(6)} + \mathbf{C}_{-2}^{(6)}\right) \\ & + B_4^6(f)\left(\mathbf{C}_4^{(6)} + \mathbf{C}_{-4}^{(6)}\right), \end{aligned} \tag{2}$$

and

$$\begin{aligned}\mathbf{H}(5d^1) = {} & \Delta_E(fd) + \zeta_{5d} s_d \cdot l_d + B_0^2(d)\mathbf{C}_0^{(2)} \\ & + B_2^2(d)\left(\mathbf{C}_2^{(2)} + \mathbf{C}_{-2}^{(2)}\right) + B_0^4(d)\mathbf{C}_0^{(4)} \\ & + B_2^4(d)\left(\mathbf{C}_2^{(4)} + \mathbf{C}_{-2}^{(4)}\right) + B_4^4(d)\left(\mathbf{C}_4^{(4)} + \mathbf{C}_{-4}^{(4)}\right), \end{aligned} \tag{3}$$

where the notation and meanings of various operators and parameters are defined according to standard practice.[34,35]

In the equations above, the spin-orbit coupling parameters for the $4f^1$ and $5d^1$ configurations (i.e., ζ_{4f} and ζ_{5d}) can be fixed and taken from Refs. 34 and 36, respectively. The parameter value of E_{avg} is always determined naturally by the whole CF splitting pattern of the $4f^1$ configuration since the parameter is introduced to shift all the $4f^1$ energy levels so that the energy of the lowest CF level is zero. The parameter $\Delta_E(fd)$ which shifts all $5d$ CF energy levels by the same amount can be adjusted to obtain the best agreement between experimental and calculated energy levels. All the crystal-field parameters (CFPs) can be evaluated in the framework of exchange charge model (ECM),[37] and the related calculation scheme can be found in the next section. Table I lists all the energy parameters used in our CF calculation.

B. Determination of CFPs based on ECM theory

A brief description of ECM is given below by following the notations used in Ref. 33 by Liu. In the framework of ECM, the CFPs of $4f$ and $5d$ electrons uniformly denoted as $B_q^k(nl)(nl = 4f \text{ or } 5d)$ [i.e., the expressions of CFPs in Eqs. (2) and (3)], can be written as a sum of two different contributions:

$$B_q^k(nl) = B_q^{(\text{pc})k}(nl) + B_q^{(\text{ec})k}(nl), \tag{4}$$

where $B_q^{(\text{pc})k}(nl)$ and $B_q^{(\text{ec})k}(nl)$ represent the contributions of point charges of all the crystal lattice ions and introduced fictitious exchange charges due to the spatial distribution of ligand electron density, respectively, as shown below:

$$B_q^{(\text{pc})k}(nl) = -e^2\langle nl|r^k|nl\rangle \sum_i q_i \beta_k (-1)^k C_{-q}^k(\theta_i,\varphi_i)/R_i^{k+1}, \tag{5}$$

$$B_q^{(\text{ec})k}(nl) = e^2 \frac{2(2k+1)}{2l+1} \sum_L S_k^{nl}(R_L)(-1)^k C_{-q}^k(\theta_L,\varphi_L)/R_L. \tag{6}$$

TABLE I. The energy parameters for Ce^{3+} ions doped in GGG and YAG, respectively, in the framework of ECM (unit: cm^{-1}). Refer to the text for their explanations.

	GGG								YAG			
	$4f$				$5d$				$5d$			
	pc[a]	ec	corr	total	pc	ec	corr	total	pc	ec	corr	total
B_0^2	−501	303	546	348	−5 750	−1 646	7188	−208	−3 382	−783	5952	1 787
B_2^2	332	136	−362	106	1 935	−86	−2419	−570	725	−786	−1276	−1 337
B_0^4	−288	−55		−343	−4 624	4 393		−231	−4 525	5 231		706
B_2^4	1407	1 133		2540	22 597	15 924		37 891	23 157	15 745		38 902
B_4^4	−774	−583		−1357	−12 427	−13 908		−26 335	−12 555	−14 187		−26 742
B_0^6	−696	−872		−1568								
B_2^6	250	412		662								
B_4^6	292	429		721								
B_6^6	231	362		593								
$G(O_1)$		4.84				1.11				1.11		
$G(O_2)$		4.97				1.63				1.63		
α		−1.09				−1.25				−1.76		
E_{avg}		1612				1 612				1 873		
$\Delta E(fd)$						36 187				40 227		
ξ		609				1 082[b]				1 082[b]		

[a]The abbreviations pc, ec, and corr stand for the CFP contributions from point charges, exchange charges, and the correction due to other factors, such as dipoles, respectively, and then total represents their sum.
[b]Reference 36.

Here C^k_{-q} is the spherical function with rank k and order $-q$ defined by Wybourne,[32] the indices i and L are used to enumerate all crystal lattice ions and ligand ions, respectively, in the nearest-neighbor coordination shell, and $(R_i, \theta_i, \varphi_i)$ and $(R_L, \theta_L, \varphi_L)$ are the spherical coordinates of the ith crystal lattice ion with the net charge eq_i and the Lth ligand ion in the reference system centered at the Ce^{3+} ion.

In Eq. (5) $\langle nl|r^k|nl\rangle$ is the radial integral of r^k between nl orbitals of the Ce^{3+} ion, which can be calculated using the numerical $4f$ and $5d$ radial wave functions of free Ce^{3+} ions provided by the standard atomic-physics codes of Cowan,[38] as shown in Ref. 39. The reduction factor β_k ($k = 2,4,\ldots,2l$) is defined as $(1-\sigma_k)$ (where σ_k is the shielding constant[40,41]) and takes into account the effects of screening of $4f$ electrons by the outer $5s^25p^6$ shell, but for the $5d$ electron it is set to 1. The ion charges q_i for GGG/YAG hosts were fixed as $+3(Gd^{3+}/Y^{3+})$, $+3(Ga^{3+}/Al^{3+})$, and $-2(O^{2-})$, correspondingly, as follows from the chemical formula and formal valences of all ions.

The exchange charge term, i.e., Eq. (6), is directly proportional to the following quadratic forms of various overlap integrals between the nl orbitals of the central Ce^{3+} ion and the outer $2p$ and $2s$ orbitals of oxygen ions:

$$S^{nl}_k(R_L) = G^{nl}_s S^{nl}_s(R_L)^2 + G^{nl}_\sigma S^{nl}_\sigma(R_L)^2 + \gamma^{nl}_k G^{nl}_\pi S^{nl}_\pi(R_L)^2, \tag{7}$$

where $\gamma^{4f}_2 = 3/2$, $\gamma^{4f}_4 = 1/3$, $\gamma^{4f}_6 = -3/2$, $\gamma^{5d}_2 = 1$ and $\gamma^{5d}_4 = -4/3$; $S^{nl}_s(R_L) = \langle nl\ 0|\ 2s0\rangle$, $S^{nl}_\sigma(R_L) = \langle nl\ 0|\ 2p0\rangle$, and $S^{nl}_\pi(R_L) = \langle nl\ \pm 1|\ 2p \pm 1\rangle$ (here the $|nlm\rangle$ notation is employed, where n, l, and m are, respectively, the principle, orbital, and magnetic quantum numbers); the G^{nl}_s, G^{nl}_σ, and G^{nl}_π entries are dimensionless adjustable parameters, which very often can be approximated to a single value, i.e., $G^{nl}_s = G^{nl}_\sigma = G^{nl}_\pi = G$. The overlap integrals between $4f/5d$ orbitals of Ce^{3+} ions and $2s/2p$ orbitals of oxygen ions for various interionic distances were numerically calculated, with the $2s$ and $2p$ radial wave functions of the oxygen ion taken from Ref. 42. The calculated dependences of the overlap integrals on the interionic distance can be fitted to the following formula:

$$S^{nl}_t(R_L) = a(R_L - b)\exp(-cR_L)R^n_L \quad (t = s,\ \sigma \text{ or } \pi) \tag{8}$$

for $0 < R_L < 10$ a.u. The fitting parameter values (a, b, c, and n) are listed in Table II.

It is generally realized that the second-order CFPs are less accurately determined by this model, as pointed out by Ref. 33, because the long-range electrostatic interaction determining the CFPs with $k = 2$ cannot be accurately calculated due to very slow convergence of the corresponding crystal lattice sums. This suggests that the contributions caused by the point dipole and quadrupole moments ignored in the original model must be considered. However, such correction calculation is very complicated, as shown by Eremin.[43] Thus, we propose a simple relation, linear with the point charge contribution, to approximate the electrostatic correction to the second-order CFPs as follows:

$$B^{(\mathrm{corr})2}_q(nl) = \alpha B^{(\mathrm{pc})2}_q(nl), \tag{9}$$

TABLE II. The values of the fitting parameter a (dimensionless), b (a.u.), c (a.u.$^{-1}$), and n (dimensionless) used in the constructed formula Eq. (8) for the calculated dependences of overlap integrals between the $2s$ and $2p$ orbitals of the oxygen ion and the $4f/5d$ orbitals of the Ce^{3+} ion on the interionic distance.

	$4f$	$5d$
a_s	1.24783	0.41410
b_s	1.16708	−0.89658
c_s	1.90106	1.44528
n_s	2.16972	2.64021
a_σ	−0.75304	−0.99616
b_σ	1.80304	2.49277
c_σ	1.59584	1.23854
n_σ	1.79939	2.06605
a_π	1.13834	1.11348
b_π	0.10336	−0.28061
c_π	1.45377	1.23219
n_π	0.59915	1.20503

where α is a fitting parameter and usually seems to be negative due to negative interaction between the dipole of the lattice ion and the $4f/5d$ electron of Ce^{3+}.

Based on the known geometry structures of GGG and YAG and the appropriate choice of the G and α values, the $4f$ and $5d$ CFPs of Ce^{3+} ions doped into GGG and YAG, respectively, can be estimated by applying Eqs. (4)–(9). More details related to these calculations can be found in Sec. V.

C. Simulation scheme of the $4f$-$5d$ absorption spectrum

For the simulation of the $4f$-$5d$ broad band structures we adopted directly the simple model proposed by Reid *et al.*,[44,45] where the areas beneath the absorption bands are proportional to the calculated oscillator strengths and the broad absorption bands are reproduced by using Gaussian shaped curves with a full width at half maximum E_{width}, displaced from the zero-phonon lines by E_{shift}. The simulation parameters E_{shift} and E_{width} can be further expressed based on the configurational coordinate model[46]

$$\begin{aligned} E_{\mathrm{shift}} &= (S - 1/2)\hbar\omega, \\ E_{\mathrm{width}} &= 2.36 \cdot \hbar\omega\sqrt{S}, \end{aligned} \tag{10}$$

where S is the Huang-Rhys factor and $\hbar\omega$ is the average energy of local phonon modes around the Ce^{3+} ion. Our recent work[26] has revealed that the effective phonon energy and the Huang-Rhys factor in GGG doped with Ce^{3+} ions are 350 cm^{-1} and 7.5, respectively. Thus, the values used in the present calculation are $E_{\mathrm{shift}} = 2450$ cm^{-1} and $E_{\mathrm{width}} = 2262$ cm^{-1}. All the energy level and intensity calculations and spectral simulations employed the extended f-shell programs written by Reid.

V. DISCUSSION

A. Energy levels of $4f^1$ and $5d^1$ configurations

The low temperature transmission spectra of GGG:Ce (1.2%) shown in Figs. 3, 4(a), and 4(b) reveal only transitions

TABLE III. The $4f$ and $5d$ CF energy levels of Ce^{3+} ions doped in GGG and YAG, respectively (data given in cm^{-1}).[a]

			GGG			YAG	
Level No.	^2L_J	I.R.	E_{calc}	E_{expt}	E_{pre}	E_{calc}	E_{ab}
1	$^2F_{5/2}$	Γ_6	0	0	0		0
2		Γ_7	160	198	163		340
3		Γ_7	722		516		800
4	$^2F_{7/2}$	Γ_6	2 116	2 145	2274		2 370
5		Γ_6	2 214	2 245	2372		2 550
6		Γ_7	2 448	2 403	2416		2 790
7		Γ_7	3 621	3 639	3400		4 260
8	$^2D_{3/2,5/2}$	Γ_7	21 100	21 100		24 609	24 040
9		Γ_6	26 500	26 500		30 879	31 660
10		Γ_6	43 835			49 052	48 070
11		Γ_7	48 118			52 154	52 540
12		Γ_7	49 438			53 804	54 190

[a]All CF energy states have the same Γ_5 representations in D_2 symmetry. The symbol I.R. stands for the double-value irreducible representation of the parent group of D_2 (i.e., D_{2d} point group). E_{calc} and E_{expt} correspond to the calculated and observed CF energy level values, respectively, whereas E_{ab} and E_{pre} represent the calculation values given by the first-principle work[24] and those predicted by directly scaling the CFPs of Eu^{3+} ions in GGG[47] by the ratio between the CF strengths[48] with the same k rank of Ce^{3+} and Eu^{3+} ions in LaF_3 host,[34] respectively.

from the lowest CF energy level of the ground $^2F_{5/2}$ state, in contrast to the room temperature spectra (see Fig. 2), which also contain transitions from the thermally populated, higher-lying level of the ground $^2F_{5/2}$ state. The line located at 3441 cm^{-1} is an example of such a hot line and is assigned to the transition between the second and the highest $4f$ energy levels. In addition, at room temperature the lines are thermally broadened, which makes their interpretation more difficult. The low temperature spectra consist of at least eight major intensity lines which can be interpreted as the transitions from the lowest level of the ground $^2F_{5/2}$ state to the four levels of the excited $^2F_{7/2}$ state in two nonequivalent Ce^{3+} centers. In addition to these most intense lines several others can be also distinguished, which are associated with Ce^{3+} centers of lower concentrations. The highest energy line is located at 3679 cm^{-1}, close to the more intense group of lines with a peak at 3638 cm^{-1} [see Fig. 4(b)]. These lines are associated with the highest energy levels of the $^2F_{7/2}$ state of several Ce^{3+} centers in GGG. The other lines, related to the remaining three levels of the $^2F_{7/2}$ state, are located between 2100 and 2450 cm^{-1} [see Fig. 4(a)].

The $4f$ energy level positions extracted from the observed $4f$-$4f$ transition spectra are collected in Table III. To confirm the rationality of our assignment, we implemented a CF calculation to predict the $4f$ energy diagram of Ce^{3+} ions in GGG, where CFPs were obtained by directly scaling those of Eu^{3+} ions in GGG[47] by the ratio between the CF strengths[48] with the same k rank determined for Ce^{3+} and Eu^{3+} ions in the LaF_3 host.[34] The predicted $4f$ CF splitting pattern, as listed in Table III, is consistent with our assignment.

The CF calculation based on ECM was made to approximately fit the observed $4f$ energy levels, where a large cluster consisting of 35 893 ions centered at the Gd site was generated in terms of the crystal structure data for GGG from Ref. 23 to ensure proper convergence of crystal lattice sums when calculating the contribution from the point charges of crystal lattice ions; two G parameters, i.e., G(O1) and G(O2) were used due to two kinds of oxygen ligands with different Gd-O distances. The calculated $4f$ energy levels based on ECM are listed in Table III for comparison with the observed and predicted values, whereas the calculated CFPs and the parameters G and α used in ECM are collected in Table I, where various contribution to CFPs are also demonstrated. The value of α is negative as we expect. The fitted $4f$ spin-orbit coupling parameter is very close to that obtained in YGG:Ce^{3+} (616 cm^{-1}).[14] The CF calculation based on ECM gives a satisfactory description of the observed $4f$-$4f$ spectrum.

The absorption spectrum of the GGG:Ce^{3+} crystal in the region of cerium f-d interconfigurational transitions at 10 K, shown in Fig. 5, consists of two relatively broad absorption bands with maxima at 426 and 346 nm. The $5d^1$ configuration of Ce^{3+} ion under D_2 symmetry is split into five CF energy levels, but only transitions to the lowest two of them can be observed. This means the other three CF energy levels are buried in the VC transition region, which makes it impossible to fit the observed data directly. However, the $5d$ energy levels of Ce^{3+} ions in YAG are known and have been predicted by the first-principle work of Garcia *et al.*[24] Because of the similarity between local structures for the Ce^{3+} ion in YAG and GGG the $5d$ energy levels of Ce^{3+} ions in YAG listed in Table III were fitted first, and the G and α values obtained were used as a starting point for the case of GGG. In the ECM calculation for YAG a large cluster consisting of 35 893 ions centered at the Y site was generated with use of the crystal structure data for YAG.[49] The calculated five $5d$ CF energy levels agree with the results given by the first-principle work very well, as Table III shows. After the G and α parameter values obtained from YAG calculation were applied to the GGG calculation, we found that the energy splitting between the lowest two CF energy levels is larger than the observed one. Such disagreement originates from the unreasonable estimation of the $5d$ second-rank CF parameters. This can be explained by the fact that the local coordination environment of the Ce^{3+} ion is characterized by a considerable distortion from the cubic O_h symmetry and this deviation generates the $5d$ second-rank CF terms with consequent energy splitting between the lowest two $5d$ CF energy levels corresponding to E representation of the ideal cubic O_h symmetry. Therefore, the α parameter controlling the $5d$ second-rank CFPs has to be slightly adjusted to obtain an agreement with experimental results of GGG. The calculated $5d$ energy levels based on ECM for GGG are collected in Table III together with the two observed CF energy levels. The absorption maximum of the calculated third $5d$ CF energy level is expected to occur at as the pure energy level position plus half of the Stokes shift, i.e., 46 285 cm^{-1} (216 nm), This energy is larger than the band gap energy (225 nm), which is consistent with the experiment. It is seen from Table III and Fig. 4 that very good agreement has been obtained. All the calculated $5d$ CFPs for YAG and GGG and the related G and α parameters were listed in Table I for comparison.

B. $4f$-$5d$ absorption intensity simulation and its temperature dependence

The measured temperature dependence of the $4f$-$5d$ absorption spectra of GGG:Ce^{3+} is shown in Fig. 3 from 10 to 400 K. The intensity of the absorption band peaked at 346 nm gradually increases with increase of temperature at the expense of the absorption band at 426 nm, which is found to decrease. In the $4f$ configuration of the Ce^{3+} ion in GGG, the lowest sublevel is separated by 160 cm^{-1} from the next higher-lying sublevel (see Table III), and thus the latter can be thermally populated in the range of temperatures studied in our experiment due to the relatively small energy difference. This can be used to explain the presently observed temperature dependence.

The absorption band intensity can be described using the following definition:[50]

$$I \propto \int \alpha(\upsilon) d\upsilon \propto P \propto S\upsilon, \tag{11}$$

where I is the absorption band intensity, α is the absorption coefficient measured in absorption spectrum, ν is the wave number of the absorption light, and P and S are the absorption oscillator and line strengths of the transition related to the absorption band, respectively. Figures 5 and 6 show the temperature dependence of the relative values of the absorption intensities of both $4f$-$5d$ transitions bands obtained with use of Eqs. (12). Based on the consideration of the thermal population of the second higher-lying sublevel and the depopulation of the lowest sublevel, the two f-d absorption band intensities can be further expressed as

$$\begin{aligned} I(346\text{ nm}) &= A_{346}\frac{S_{19}\vartheta_{19} + S_{29}\vartheta_{29}\exp\left(-\frac{\Delta E}{k_B T}\right)}{1+\exp\left(-\frac{\Delta E}{k_B T}\right)}, \\ I(426\text{ nm}) &= A_{426}\frac{S_{18}\vartheta_{18} + S_{28}\vartheta_{28}\exp\left(-\frac{\Delta E}{k_B T}\right)}{1+\exp\left(-\frac{\Delta E}{k_B T}\right)}, \end{aligned} \tag{12}$$

where S_{ij} and ν_{ij}, respectively, represent the $4f$-$5d$ transition line strength and energy between energy levels i and j (here i and j are the labeling of energy levels used in Table III), ΔE is the energy difference between energy levels 1 and 2, k_B is the Boltzmann constant, and T is the temperature. The A_{ij} are adjustable empirical parameters of proportionality. The parameters S_{ij} andν_{ij} involved in Eqs. (12) were calculated based on the $4f$ and $5d$ CF eigenvalues and eigenvectors obtained by diagonalization of the effective parametrized Hamiltonian matrices for two configurations, and tabulated in Table IV. ΔE was taken as the calculated value, i.e., 160 cm^{-1} (see Table III). Resulting theoretical dependencies are shown in Fig. 6 as broken lines.

A fit of Eqs. (12) to the experimental data, treating all S_{ij} and ΔE as adjustable parameters, is shown as solid lines in Fig. 6. The experimental line strength S_{ij} parameters obtained from the fit are listed in Table IV.

It is seen from Fig. 6 that our theoretical prediction reproduces the experimental results very well. The vibronic bands of $4f$-$5d$ transitions at the different temperatures can be also simulated by employing the scheme referred in Sec. IV C and the temperature dependence function of the absorption band intensity [i.e., Eqs. (12)]. The simulated absorption spectra at the different temperatures were plotted in Fig. 5 for comparison with the measured ones. Figure 5 also shows a very good agreement between theory and experiment, which confirms the reliability of our CF calculation based on ECM.

TABLE IV. The calculated $4f$-$5d$ line strengths and transition energies between the lowest two CF energy levels of $4f^1$ configuration and those of $5d^1$ configuration.[a]

$4f$-$5d$ absorption	Line strength experimental	S_{ij} ($\times 10^{20}$ cm^2) theoretical	Transition energy ν (cm^{-1})
$1 \rightarrow 8$	35.7 ± 0.2	35.81748	21 100
$1 \rightarrow 9$	7.5 ± 0.1	7.50315	26 500
$2 \rightarrow 8$	6.1 ± 1.1	5.21194	20 940
$2 \rightarrow 9$	30.5 ± 0.5	38.20143	26 340

[a]The radial integral between $4f^1$ and $5d^1$ configurations $\langle 5d|r|4f\rangle$ is taken as 0.284 Å.[51]

VI. CONCLUSIONS AND SUMMARY

Low temperature infrared absorption of GGG:Ce^{3+} shows evidence of multicenter structure of this dopant in garnet host. At least two major types of Ce^{3+} centers are observed, along with others of lower concentration. Very large splitting of the excited $^2F_{7/2}$ state of Ce^{3+} is observed, which comes from the influence of spin-orbit interaction resulting from level mixing due to small separation between the ground and excited states in $4f^1$ configuration. The highest energy state is located at about 3700 cm^{-1} above the lowest energy state.

Theoretical crystal field calculations with use of exchange charge model, assuming that the Ce^{3+} ions substitute Gd^{3+} in the GGG host, allow us fit the experimentally observed Ce^{3+} absorption lines of the highest intensity, with very good accuracy. The fit of the other lines was not attempted since the nature of the Ce^{3+} centers associated with these lines is not known and awaits further studies. Small adjustment of the CF parameters would allow fitting the observed energies, however such a procedure would not allow explaining of the origin of the observed Ce centers. Their nature may be associated with the so called antisites of cations in garnet host (substitution of octahedral sites, in which Ga ions are located) or influence of closely located defects of the structure, associated with cation or anion (oxygen) nonstoichiometry of garnets[22] or nonintentional dopants. Influence of similar defects was considered in the case of YAG:Ce by Muñoz-García *et al.*[52]

The Ce^{3+} ions in GGG host substitute Gd ions in dodecahedral sites with D_2 symmetry. All f^n states with odd n in D_2 symmetry have the same Γ_5 representations.[53] However, at certain conditions, for example by application of external pressure, examined by us in Ref. 25, the symmetry of the GdO_8 molecule became close to D_{2d}. Doping with cations with ionic radii different than that of Gd^{3+} can lead to the similar geometry. In the D_{2d} symmetry the $^2F_{5/2}$ state splits into levels with Γ_6 and Γ_7 representations. The electrical dipole transitions are allowed between the states with different representation in this symmetry, the transitions between the states with the same symmetry are forbidden. Spin-orbit interaction mixes pure electronic states and partially releases

these strict selection rules, however they still strongly influence the absorption properties of cerium dopant in garnets.

Studies of the temperature dependence of the $4f$-$5d$ absorption of Ce in GGG show the importance of the selection rules for the optical transitions in this system. Apparently, the transitions from the ground state of the $4f^1$ configuration to the first level (level 8 in our notation) of the $5d^1$ are more probable than to the second level (level 9), as it could be seen in Table IV. A reverse situation is valid for the transitions from the higher-lying second level on the ground state, separated from the lowest-lying level by about 160 cm^{-1}. This is a result of the influence of the selection rules. As it can be seen in Table III, the lowest level of the ground $^2F_{5/2}$ state has Γ_6 symmetry, and the second one Γ_7. Since the irreducible representations of the lowest two $5d^1$ levels have the opposite order, the allowed transitions are between levels $1 \rightarrow 8$ and $2 \rightarrow 9$, and are forbidden between levels $1 \rightarrow 9$ and $2 \rightarrow 8$. This agrees very well with observed probabilities of the absorption transitions between $4f^1$ and $5d^1$ configurations, shown in Table IV. A small separation between the first two levels of the ground state allows the second level to be thermally populated at relatively low temperatures and it is responsible for the changes of the intensity of the two $4f$-$5d$ bands of Ce ions between helium and room temperature.

Selection rules appropriate for this symmetry are also the most probably responsible for the observed lack of luminescence transitions between the first level of the $5d^1$ configuration (level 8) and the highest-lying level of the $4f^1$ configuration (level 7) since their group-theory representations are the same. Usually, in garnets luminescence is only observed for transitions from level 8 to the lower located levels (levels 1–6) of the $^2F_{5/2}$ state since there are levels characterized by a different representation than that of level 8 (see Table III). Such a situation was also observed by us in the high-pressure studies of GGG:Ce.[26]

Finally, we would like to mention that most of the conclusions of this paper are also valid for the more important in view of application, YAG:Ce and Ce doped mixed crystals, based on YAG.

ACKNOWLEDGMENTS

The cooperation program between Estonian and Polish Academies of Sciences for the years 2009–2012 is kindly acknowledged. This work was partially supported by the European Union within the European Regional Development Fund through the Innovative Economy grant MIME (POIG.01.01.02-00-108/09).

[1] S. Kück, Appl. Phys. B **72**, 515 (2001).
[2] A. A. Kaminskii, Laser Photon. Rev. **1**, 93 (2007).
[3] J. M. Robertson, M. W. Van Tol, W. H. Smits, and J. P. H. Heynen, Philips J. Res. **36**, 15 (1981).
[4] B. Hüttl, U. Troppenz, K. O. Velthaus, C. R. Ronda, and R. H. Mauch, J. Appl. Phys. **78**, 7282 (1995).
[5] E. Danielson, M. Devenney, D. M. Giaquinta, J. H. Golden, R. C. Haushalter, E. W. McFarland, D. M. Poojary, C. M. Reaves, W. H. Weinberg, and X. D. Wu, Science **279**, 837 (1998).
[6] J. L. Wu, G. Gundiah, and A. K. Cheetham, Chem. Phys. Lett. **441**, 250 (2007).
[7] J.-G. Kang, M.-K. Kim, and K.-B. Kim, Mater. Res. Bull. **43**, 1982 (2008).
[8] Y.-P. Fu, S.-B. Wen, and C.-S. Hsu, J. Alloys Compd. **458**, 318 (2008).
[9] M. Balcerzyk, Z. Gontarz, M. Moszynski, and K. Kapusta, J. Lumin. **87-89**, 963 (2000).
[10] M. Nikl, Meas. Sci. Technol. **17**, R37 (2006).
[11] G. Blasse and A. Bril, J. Chem. Phys. **47**, 5139 (1967).
[12] R. R. Jacobs, W. F. Krupke, and M. J. Weber, Appl. Phys. Lett. **33**, 410 (1978).
[13] D. J. Robbins, B. Cockayne, B. Lent, C. N. Duckworth, and J. L. Glasper, Phys. Rev. B **19**, 1254 (1979).
[14] G. F. Herrmann, J. J. Pearson, and K. A. Wickersheim, J. Appl. Phys. **37**, 1312 (1966).
[15] B. F. Aull and H. P. Jenssen, Phys. Rev. B **34**, 6640 (1986).
[16] J. Andriessen, P. Dorenbos, and C. W. E. van Eijk, Phys. Rev. B **72**, 045129 (2005).
[17] D. Sugak, A. Matkovskii, A. Durygin, A. Suchocki, I. Solskii, S. Ubizskii, K. Kopczynski, Z. Mierczyk, and P. Potera, J. Lumin. **82**, 9 (1999).
[18] S. Chénais, F. Druon, F. Balembois, P. Georges, A. Brenier, and G. Boulon, Opt. Mater. **22**, 99 (2003).
[19] D. Galanciak, M. Grinberg, W. Gryk, S. Kobyakov, A. Suchocki, G. Boulon, and A. Brenier, J. Phys.: Condens. Matter **17**, 7185 (2005).
[20] B. Jiang, Z. Zhao, J. Xu, and P. Deng, J. Cryst. Growth **268**, 135 (2004) .
[21] S. Kück, K. Petermann, U. Pohlmann, and G. Huber, J. Lumin. **68**, 1 (1996).
[22] A. Brenier, A. Suchocki, C. Pedrini, C. Madej, and G. Boulon, Phys. Rev. B **46**, 3219 (1992).
[23] J. Sasvári and P. E. Werner, Acta Chem. Scand. A **37**, 203 (1983).
[24] J. Gracia, L. Seijo, Z. Barandiarán, D. Currlla, H. Niemansverdriet, and W. Van Gennip, J. Lumin. **128**, 1248 (2008).
[25] A. Kaminska, R. Buczko, W. Paszkowicz, H. Przybylińska, E. Werner-Malento, A. Suchocki, M. Brik, A. Durygin, V. Drozd, and S. Saxena, Phys. Rev. B **84**, 075483 (2011).
[26] A. Kaminska, A. Duzynska, M. Berkowski, S. Trushkin, and A. Suchocki, Phys. Rev. B **85**, 155111 (2012).
[27] G. H. Dieke, *Spectra and Energy Levels of Rare Earth Ions in Crystals* (Interscience, New York, 1968).
[28] W. Nie, G. Boulon, and A. Montail, Chem. Phys. Lett. **164**, 106 (1989).
[29] C. R. Stanek, K. J. McClellan, M. R. Levy, C. Milanese, and R. W. Grimes, Nucl. Instrum. Methods Phys. Res., Sect. A **579**, 27 (2007).
[30] S. P. Feofilov, A. B. Kulinkin, T. Gacoin, G. Mialon, G. Dantelle, R. S. Meltzer, and C. Dujardin, J. Lumin. **132**, 3082 (2012).
[31] A. J. Wojtowicz, M. Kazmierczak, A. Lempicki, and R. H. Bartram, J. Opt. Soc. Am. B **6**, 1106 (1989).
[32] B. G. Wybourne, *Spectroscopic Properties of Rare Earths* (Interscience, New York, 1965).

[33]G. K. Liu, in *Spectroscopic Properties of Rare Earths in Optical Materials*, edited by G. K. Liu and B. Jacquier (Tsinghua University Press and Springer, Berlin, 2005).
[34]W. T. Carnall, G. L. Goodman, K. Rajnak, and R. S. Rana, J. Chem. Phys. **90**, 3443 (1989).
[35]M. F. Reid, L. van Pieterson, R. T. Wegh, and A. Meijerink, Phys. Rev. B **62**, 14744 (2000).
[36]M. F. Reid, L. van Pieterson, and A. Meijerink, J. Alloys Compd. **344**, 240 (2002).
[37]B. Z. Malkin, in *Spectroscopy of Solids Containing Rare Earth Ions*, edited by A. A. Kaplyanskii and R. M. Macfarlane (North-Holland, Amsterdam, 1987), p. 13.
[38]R. D. Cowan, *The Theory of Atomic Structure and Spectra* (University of California Press, Berkeley, 1981).
[39]G. W. Burdick and M. F. Reid, in *Handbook on the Physics and Chemistry of Rare Earths*, edited by K. A. Gschneidner, Jr. and L. Eyring (North-Holland, Amsterdam, 2007), Vol. 37, p. 61.
[40]R. M. Sternheimer, M. Blume, and R. F. Peierls, Phys. Rev. **173**, 376 (1968).
[41]S. Edvardsson and M. Klintenberg, Mater. Sci. Forum **315**, 407 (1999).
[42]E. Clementi and C. Roetti, At. Data Nucl. Data Tables **14**, 177 (1974).
[43]V. V. Iglamov and M. V. Eremin, Phys. Solid State **49**, 229 (2007).
[44]L. van Pieterson, M. F. Reid, R. T. Wegh, S. Soverna, and A. Meijerink, Phys. Rev. B **65**, 045113 (2002).
[45]L. van Pieterson, M. F. Reid, G. W. Burdick, and A. Meijerink, Phys. Rev. B **65**, 045114 (2002).
[46]B. Henderson and G. F. Imbusch, *Optical Spectroscopy of Inorganic Solids* (Clarendon, Oxford, 1989).
[47]J. B. Gruber, U. V. Valiev, G. W. Burdick, S. A. Rakhimov, M. Pokhrel, and D. K. Sardar, J. Lumin. **131**, 1945 (2011).
[48]F. Auzel and O. L. Malta, J. Phys. (France) **44**, 201 (1983).
[49]T. S. Chernaya, L. A. Muradyan, V. A. Sarin, E. M. Uyukin, Kh. S. Bagdasarov, and V. I. Simonov, Kristallografiya **34**, 1292 (1989).
[50]C. Görller-Walrand and K. Binnemans, in *Handbook on the Physics and Chemistry of Rare Earths*, edited by K. A. Gschneidner, Jr. and L. Eyring (North-Holland, Amsterdam, 1998), Vol. 25, p. 101.
[51]T. Chen, C. K. Duan, and S. D. Xia, J. Alloys Compd. **439**, 363 (2007).
[52]A. Belén Muñoz-García, E. Artacho, and L. Seijo, Phys. Rev. B **80**, 014105 (2009).
[53]G. F. Koster, J. O. Dimmock, R. G. Wheeler, and H. Statz, *Properties of the Thirty-Two Point Groups* (MIT Press, Cambridge, MA, 1963).